



Article citation info:

Jackowski J, Żmuda M, Wiczorek M, Comparative analysis of small size non-pneumatic tires and pneumatic tires - radial stiffness and hysteresis, selected parameters of the contact patch. *Eksploracja i Niezawodność – Maintenance and Reliability* 2023; 25(3) <http://doi.org/10.17531/ein/167362>

Comparative analysis of small size non-pneumatic tires and pneumatic tires - radial stiffness and hysteresis, selected parameters of the contact patch

Indexed by:



Jerzy Jackowski^a, Marcin Żmuda^{a,*}, Marcin Wiczorek^a

^a Military University of Technology, Warsaw Poland

Highlights

- The radial stiffness, hysteresis, contact patch of non-pneumatic (NPTs) and pneumatic tires (PTs) were compared.
- NPTs have a higher radial stiffness compared to PTs.
- The flexible cell structure increases the energy losses associated with the vertical displacements of the axle of the NPT.
- NPTs have a shorter length of the contact patch and the shape of the tread area allows to change the width of the contact patch.

Abstract

Nowadays, non-pneumatic tires are becoming an increasingly likely alternative to pneumatic tires. The function of compressed air has been taken over by the belt and the elastic structure (materials used and shape of the components). The research presented in the paper was carried out in quasi-static conditions. The research's aim was to compare the radial stiffness, hysteresis and selected parameters of the contact patch of two non-pneumatic tires and four pneumatic tires used interchangeably in ATVs/UTVs. The analyzed non-pneumatic tires are characterized by greater radial stiffness than pneumatic tires of the same size. Moreover the wheel with a cellular structure has the highest hysteresis of the radial characteristics of the tested wheels and the highest values of the unit pressure in the area of contact patch. The paper also verified two methods of calculating the contact patch length of non-pneumatic tires.

This is an open access article under the CC BY license (<https://creativecommons.org/licenses/by/4.0/>)

Keywords

non-pneumatic tires/wheels, pneumatic tires/wheels, radial stiffness, hysteresis, contact patch, average value of pressures in the contact patch

1. Introduction

Nowadays construction of non-pneumatic tires (NPTs) reflect the properties of pneumatic tires (PTs) without the need to maintain liquid or gaseous substances inside them under a certain pressure [1]. These solutions are protected by patent law or published in the form of scientific research results, most often as the results of numerical calculations/simulations. Few companies have decided to introduce non-pneumatic tires in the market offer or present this type of construction as a technology demonstrator.

A detailed analysis of the most common construction solutions of NPTs is presented in [39, 35]. In the construction of such the wheel, the following components are always detailed: rim, elastic structure, belt with a core and tread. The NPT's tread

and rim perform the same tasks as in the case of pneumatic tires. The belt consists of inextensible membranes with a core between them. The elastic structure connects the wheel rim with the belt. This component of non-pneumatic tires most often occurs in the form of radial spokes or as interconnected geometric figures (referred to as a cellular or layered structure). It is also responsible for the mechanism of carrying multidirectional loads, including vertical forces. It follows that the function of the compressed air of a pneumatic tire in the NPT is mimic jointly by the elastic structure and the belt. The elasticity of those two components causes deformation (flattening) of the belt with the core in the contact patch when the wheel axle is loaded. The remaining non-deformed part

(*) Corresponding author.

E-mail addresses:

J. Jackowski (ORCID: 0000-0002-5787-1451) jerzy.jackowski@wat.edu.pl, M. Żmuda (ORCID: 0000-0002-4990-6378) marcin.zmuda@wat.edu.pl, M. Wiczorek (ORCID: 0000-0002-0297-535X) marcin.wiczorek@wat.edu.pl

of the belt stores mechanical energy (this action is compared in [14, 15, 21] to a bow). The method and range of allowable flexibility of the elastic structure are very important for the properties of the non-pneumatic tire in the radial direction. The vertical axial displacement of the non-pneumatic tire with single spokes is limited by the possibility of stretching the spokes located outside the contact patch, because the normal load is carried by the upper, undeformed part of the wheel ("top loader"). At the same time, as a result of loading with a normal force, the elastic structure located between the contact patch and the wheel axle is compressed and deformed (buckling), which means that it can carry only a small load or no load [4, 7, 17, 39]. In addition, in this solution of elastic structure, the high stiffness of the spokes counteracted the circumferential deformations of the belt during the vertical load of the wheel, thus reducing the length of the contact patch [24]. In the case of the cellular structure, part of the vertical load is carried by the deformed structure under the wheel axle ("bottom loader") [2, 39]. Its load carrying capability is affected by incl. increasing the thickness of the components or a properly shaped structure (e.g. auxetic) [3, 8, 21]. In practice, the use of the specified NPT solution (e.g. type of elastic structure) is determined by detailed operational requirements or the target vehicle segment [33]. This is confirmed by the works presented in [34]. Simulation and experimental research were carried out there, and the process of manufacturing NPT equipped with radial spokes was described. The process of optimizing dimensions is presented, including the width and direction of the spoke. The aim was to minimize spoke weight (volume of material) and use NPT as the equivalent of a pneumatic tire on a commercial electric vehicle.

An important feature of a wheel is its radial stiffness characteristics. It illustrates the course of changes in the normal force value as a function of wheel deflection in the normal direction. At the same time, it allows to obtain information, incl. about possible wheel vibrations, rolling resistance (energy losses related to wheel/tire deformation in the radial direction), and values of loads transferred to vehicle suspension. In [6], quasi-static experimental and numerical research of the commercial NPT for UTV/ATV (Utility Terrain Vehicle/ All Terrain Vehicle) were presented. Experimental research included the determination of the radial stiffness characteristics and average values of the pressure in the contact patch of the

wheels with the rigid surface. Pressure-sensitive foil (film) was used to determine the contact patch parameters. This method of registering the shape and area of the contact patch as well as the occurring pressures required keeping the wheel loaded for about 120 s. The experiment also included variable values of the wheel camber angle. The change in the angle value reduced the radial stiffness of the wheel. The results of quasi-static research were used to validate the numerical model, which was then used to determine the dynamic characteristics of the longitudinal force as a function of wheel slip.

The results of experimental and numerical research on radial stiffness can also be found in [27], where a wheel used in a skid steer was analyzed. In numerical research, the influence of spoke thickness changes on the trajectory of the radial characteristics and the value of the stress acting on the spoke was evaluated. The results of numerical calculations made it possible to find a spoke thickness that provides radial stiffness of the wheel comparable to the pneumatic tire (which was previously selected as the goal). The next stage of research [26] was the validation of the developed numerical model using the results obtained by rolling the NPT on the drum at a speed of approx. 3 m/s. In addition, deflections of individual spokes in specific places on the circumference of the wheel were analyzed. As was shown, the numerical model was highly compatible with the experiment results and will be applied to the assessment of rolling resistance and the dynamic NPT reaction during overcoming road unevenness. In [36], a comparison of the experimental and numerical research results of a pneumatic tire with the numerical research results of three NPTs was shown. The flexible structure was differentiated by the use of radial spokes, hexagonal cell structure, and grid type. Potential differences in NPT properties have been pointed out. Those equipped with the grid type cell structure were characterized by a significant resistance to buckling (this feature was strongly marked during the tests of the radial characteristics). The NPT equipped with radial spokes, on the other hand, had lower radial stiffness compared to the pneumatic and NPT with a hexagonal cell structure.

In [5], the analysis of influence the hexagonal structure changes (its single cell), i.e. its length, width, internal angle, wall thickness, density (total number of cells) on selected wheel properties (radial deflection, energy losses, pressures in the

contact patch) was carried out. It was also shown that increasing the height of the cell increases the vertical displacement of the wheel axis (deformation of the elastic structure) during loading in the normal direction. The opposite phenomenon was observed during increasing the total number of cells (packing density) and the thickness of their walls. A similar nature of changes occurred in the area of energy losses related to the vertical deformation of the NPT. In addition, a significant concentration of pressures in the contact patch was observed at the connection point of the flexible structure with the belt, and the pressure distribution itself was significantly dependent on the length and thickness of the cell walls of the layered structure.

In [11], the influence of changing the geometric dimensions of a single hexagonal cell and its wall thickness on the radial characteristics, contact patch parameters, and rolling resistance was analyzed. It has been shown that the rolling resistance of an NPT with a cellular elastic structure depends on its volume (mass) and the range of its deformations. The lowest rolling resistance force values were obtained for the structure in which the smallest cell expanding angle was used. Increasing the wall thickness of the cell structure limited the range of vertical displacements of the NPTs. In [38], the wall thickness of a hexagonal cell was changed for three elastic NPT structures with defined dimensions and material data. The goal of this search was to obtain a radial stiffness equivalent to a pneumatic tire of size 205/55R16. The developed numerical models were also used to assess the directional stiffness of the NPTs (circumferential and lateral). Increasing the internal angle of the hexagonal cell resulted in an increase in the vertical displacements of the wheels. Higher circumferential deformations of the cellular structure (compared to pneumatic tires) resulted in a decrease in the value of the circumferential stiffness of the tested NPTs. The opposite trend was observed for the lateral direction.

Formally, the area of the NPT contact patch and the average value of the pressure in this area are shaped at the modeling stage by selecting the geometric dimensions of the NPT and the materials properties of the belt [22, 31]. It is assumed that the product of the average pressure value of the contact path and the radius of the outer layer of the belt reinforcement (approximately the outer radius of the NPT) is equal to the

product of the shear modulus and the height of the layer of the belt material (between the layers of reinforcement) for NPT equipped with a homogeneous core [4, 22]. The above indicates that the average value of the pressure is an important design criterion of the NPT, which determines, including on the properties of the material used to create the core. Therefore, the introduction of a composite core in place of the homogeneous material core is currently being considered (aimed to obtain a structure characterized by a high dynamic shear modulus G , high elongation at break, and low energy losses during deformation). This will allow to reduce its thickness while maintaining the usable properties of the wheel [31].

Research [36], conducted with the numerical models, revealed the influence of the applied elastic structure also on the contact patch and contact pressure. The analysis did not take into account the influence of the tread pattern, and a significant concentration of pressure was observed at the contact point of the elastic structure with the belt/tread. In [6], in the numerical assessment of the pressures acting in the contact patch with the rigid ground, the shape of the tread was taken into account. The parameters of the contact patch, values and pressure distribution determined in numerical tests were consistent with those determined during the experiment on the test bench.

Other specific constructions of NPTs are also described in the literature. An example may be a structure named by the creators as ME-wheel (mechanical elastic wheel) [31]. In this wheel, steel hinges/joints with a different number of components were used to connect the belt with the wheel rim. The use of three-piece hinges resulted in a reduction in circumferential stiffness compared to the results obtained for two-piece hinges. The increase in radial stiffness was also observed with the increase in the number of elements (hinges) connecting the belt with the wheel rim. The influence of the number of hinge elements on the course of the side characteristics was negligible.

The review of the literature indicates that the quasi-static characteristics of the radial stiffness, hysteresis, shape of the contact patch with the rigid ground and the value of the contact pressure are important features affecting the operational properties of the NPT (they occur individually or jointly in the cited source materials). Expensive and time-consuming experimental research [12, 28] are often replaced by numerical

research, which predominate in the available analyses. Estimated features are usually compared with one pneumatic tire or proprietary NPT constructions. In addition, in analyzes of the contact patch parameters, the tread blocks are often omitted, and when they are included, their shape is simplified and the transverse outline of the tread is omitted. Therefore, it seems reasonable to carry out a comparative analysis using detailed results of experimental research on non-pneumatic tires and pneumatic tires. This article presents the results of experimental research related to the determination of the radial stiffness characteristics and the parameters of the wheels' footprints (NPTs and PTs), which can be used interchangeably in an ATV/UTV. The research included two non-pneumatic tires with different elastic structures (single spokes and hexagonal cell) and four pneumatic tires (radial and diagonal).

2. Methodology and research objects

Experimental research was carried out on the Universal Test Bench for Quasi-Static Tire Research (fig. 1). A detailed description of the measurement capabilities of the stand was presented earlier in [13]. Experimental research included the determination of the radial stiffness characteristics, determination of energy consumption of the vertical deflection process of analyzed wheels, and measurement of the contact patch with a flat, non-deformable (rigid) ground. These research were designed to compare the important properties of commercial NPTs and their corresponding PTs. The initial comparative analysis was presented by the authors in [10], which included an analysis of the radial stiffness characteristics of NPTs and one pneumatic tire.

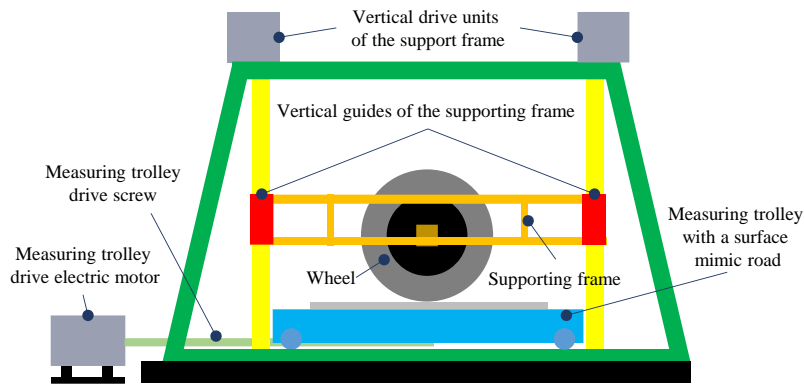


Fig. 1. Universal Test Bench for Quasi-Static Tire Research.

Table 1. Description of research objects (data taken from [16, 17, 29, 30]).

Identification mark	Tire size	Carcass plies	Ply Rating (PR)/ Load capacity index (load carrying capacity [kg])	Speed-category symbol (speed [km/h])	Maximum inflation pressure [kPa] ([psi])	Mass* [kg]	Location in the vehicle
NPT_1	26x9N14	ND	ND/69 (325)	J (100)	non apply	23,4	steering/drive axle
NPT_2	26x8.00-14	ND	ND / (325+)**	(40)**	non apply	25,4	steering/drive axle
PT_1	AT26x8-14	bias	6PR/44 (160)	N (140)	48,26 (7)	15,8	front/steering axle
PT_2	AT26x9-14	bias	6PR/65 (290)	J (100)	96,52 (14)	17,6	ND
PT_3	26x9.00R14 (225/65R14)	radial	6PR/73 (365)	N (140)	ATV – 48,26 (7) UTV – 124,10 (18)	16,8	front/steering axle
PT_4	26x9xR14	radial	10PR/77 (412)	F (80)	150 (22)	18,0	front/steering axle

- * - mass measurement of the pneumatic tires was carried out after mounting on the wheel rim, the pressure inside the tire was equal to atmospheric pressure, the measurements were made using the Universal System for Weighing Vehicles with a measuring range of 4÷600 kg and an accuracy of 0,2 kg,
- ** - load capacity and maximum speed were determined on the basis of information obtained from the distributor [29],
- ND - no data/lack of data

The selection of research objects was preceded by an analysis of the availability of commercial non-pneumatic tires. Their size and load capacity were used to indicate a group of comparative wheels made of 4 pneumatic tires. The wheels/tires accepted for testing, together with the assigned identification mark, are shown in fig. 2, and the basic features of their construction are listed in table 1.

Due to the lack of manufacturer's information regarding the NPT_2, its load capacity and maximum speed were determined on the basis of information obtained from the distributor [29] and a review of technical and operational parameters of ATVs and UTVs in which it can be used. Normal load values (table 2) were selected based on the ATV/UTV load variation range. Factors such as curb weight, payload, and expected load changes resulting from vehicle operating conditions (acceleration, braking, driving on a slope, etc.) were taken into account during determining the force values.

The selected loads for some pneumatic tires exceed the value resulting directly from their load capacity index. However, in accordance with the regulations of the Economic

Commission for Europe of the United Nations (UN/ECE) [19, 20], the load capacity index means the maximum permissible load on a pneumatic tire at a speed corresponding to the appropriate speed category symbol, while maintaining the conditions of use specified by the manufacturer. The experimental research was carried out in quasi-static conditions. According to [19, 20], the wheel load capacity index (whose linear velocity was 0 m/s) increases from 110% to 150%.

The aim of the NPTs is to mirror and replace the compressed air properties of pneumatic tires. Unfortunately, NPT manufacturers do not provide information on what value of inflation pressure of pneumatic tires is reflected by the NPT structure they use. Therefore, to conduct a comparative analysis of NPTs with PTs, it was decided to select a wide range of changes in the inflation pressure values. They were selected based on information on the maximum values of air pressure in the PTs recommended by the manufacturers (placed on the tire's sidewall). The lowest value of tire inflation pressure was assumed to be the one close to the maximum value recommended for the PT_1, and the highest maximum

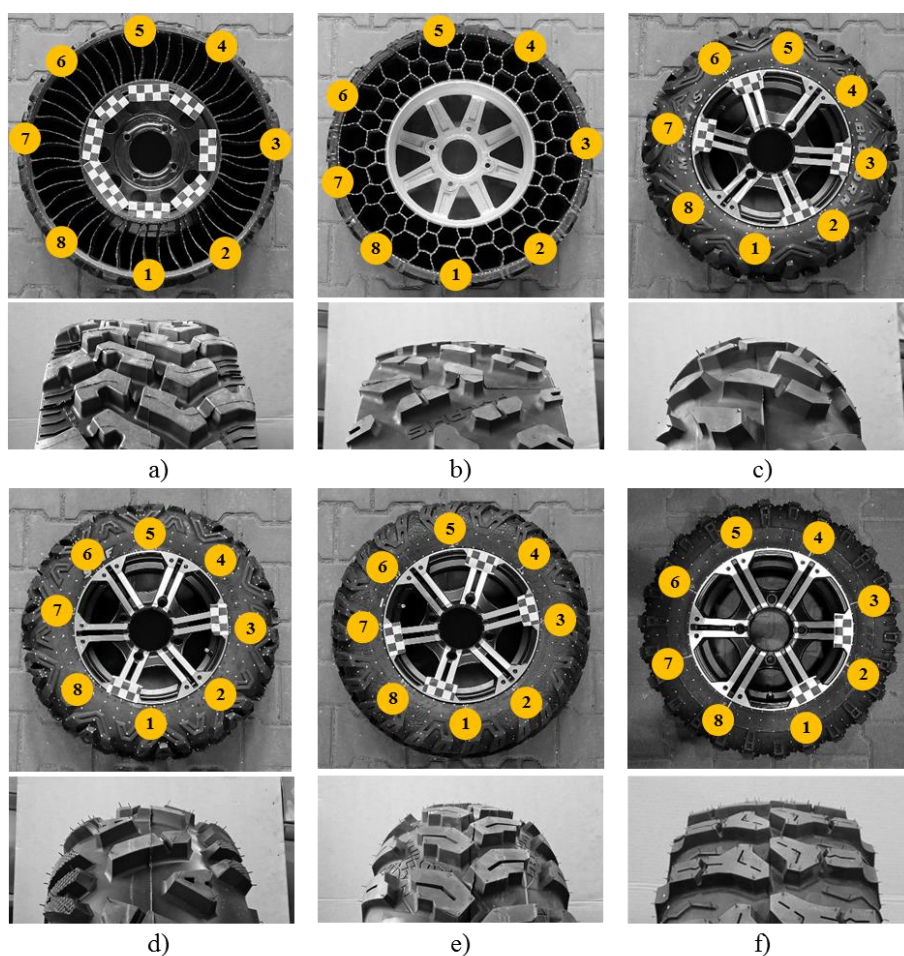


Fig. 2. Research objects/wheels: a) NPT_1, b) NPT_2, c) PT_1, d) PT_2, e) PT_3, f) PT_4.

Table 2. Experimental research conditions.

Research objects	Normal load [kN]	Inflation pressure [kPa]
NPT_1	1,00	-
NPT_2		-
PT_1	2,00	45
PT_2	3,00	45, 70, 95
PT_3	3,75*	45, 70, 95, 120
PT_4		45, 70, 95, 120, 145

* - only for contact patch determination research.

recommended value for the PT_4. The range defined in this way was divided into parts, assuming a constant value of the pressure change, which was 25 kPa, with the additional condition that the selected successive values of the inflation pressure of a given tire may not exceed those indicated by the manufacturer. This procedure provided good coverage of the research field of interest to the authors.

The radial stiffness characteristics were determined for a non-rotating wheel on a flat horizontal rigid surface. It consists in pressing the axle of the tested wheel towards the measuring surface, placed on normal force sensors (fig. 3). During the experiment, the values of axle displacement and normal force were recorded, the value of the force was changed smoothly from zero to 125% of the assumed normal load (table 2) and then reduced to zero. The obtained hysteresis loop (fig. 4) can be used to determine the amount of energy lost during the cyclic tire deformations occurring during driving. The energy losses of the research objects for the recorded force during wheel loading and unloading were expressed by the hysteresis coefficient [9]:

$$w_H = \frac{W_{load} - W_{unload}}{W_{load}} \quad (1)$$

- w_H – the hysteresis coefficient,
- W_{load}, W_{unload} – the work done in loading and unloading the wheel, respectively.

The next step was to determine the center line on the recorded hysteresis loop (fig. 4), which is the average value of the forces measured during loading and unloading with the same wheel deflection. The course of this line was used to calculate the value of the radial stiffness coefficient for the ranges corresponding to 25%, 50%, 75%, and 100% of the assumed normal load, according to the relation [18]:

$$k_{Ri} = \frac{\Delta Z_K}{\Delta u_z} \quad (2)$$

- k_{Ri} – radial stiffness coefficient for the i-th range,
- ΔZ_K – increase in the value of the normal load acting on the wheel axis,
- Δu_z – increase in the radial deflection of the wheel.

In order to increase the credibility of the obtained results and to comprehensively capture the properties of the analyzed wheels, the measurement of the radial characteristics was carried out in eight, evenly distributed locations (cross-sections) around the circumference of the wheel (approx. every 45°). In addition, the research in the assumed cross-section and set conditions were repeated three times, always starting with the load with the highest value (this was to standardize the impact of the Mullins effect, which is characteristic especially for NPTs). The values of the radial stiffness coefficients of the eight analyzed cross-sections were used to calculate the radial stiffness non-uniformity on the circumference of the wheel [40]:

$$N_{kR} = \frac{k_{Rmax} - k_{Rmin}}{k_{Rave}} \quad (3)$$

- k_{Rmax} – maximum value of radial stiffness coefficient on the circumference of the research object,
- k_{Rmin} – minimum value of radial stiffness coefficient on the circumference of the research object,
- k_{Rave} – the average value of the radial stiffness on the circumference of the research object (from eight measurement locations).

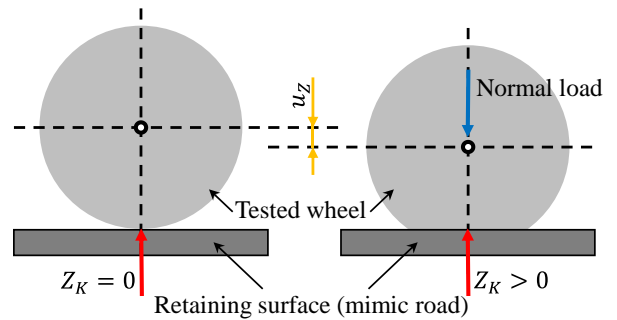


Fig. 3. Principle of measurement of radial stiffness characteristics.

The next test was to determine the wheel contact patch on the rigid ground and to determine the changes occurring under the influence of normal load. In this test, an observation window was used, made of glass of appropriate thickness, to which the research object was pressed with the assumed value of normal load (fig. 5). In order to facilitate registration, the window surface against which the object was pressed during the test was

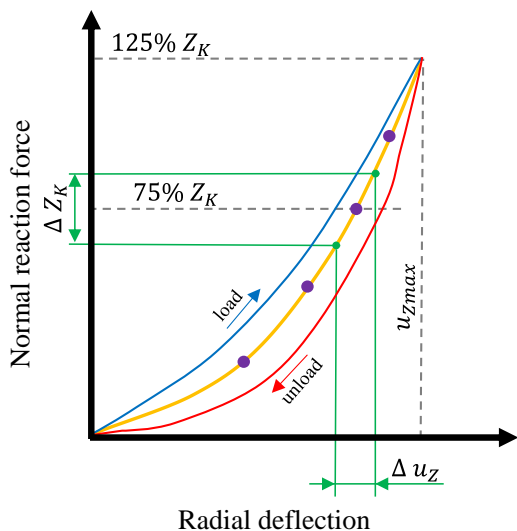


Fig. 4. Methodology for determining the radial stiffness coefficients for the i -th range of normal load.

wetted with water with the addition of a surfactant. The contact patch was recorded with a camera three times in each of the two places (cross-sections) on the circumference of the wheel located 90° to each other (this change was dictated by the desire to take into account the differentiation of the tread pattern). The resulting images were then analysed using graphics software. Changes in the average value of the contact pressure and the area of the contact patch as a function of the normal load were analysed.

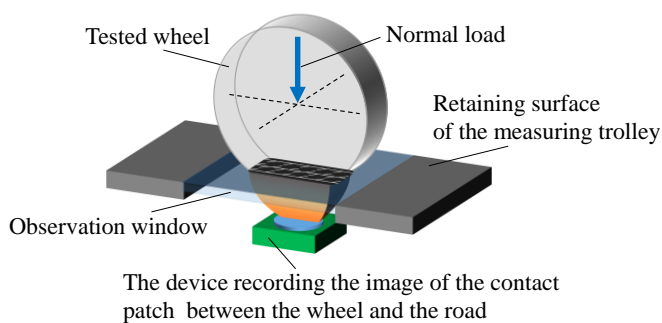


Fig. 5. Method of registering the wheel contact path with the rigid ground.

Knowledge of the actual area of the wheel contact patch with the ground and the normal load values made it possible to determine the average value of the pressure exerted by the tread blocks [32]:

$$q_{ave} = \frac{Z_K}{A_W} \quad (4)$$

- q_{ave} – the average value of the contact pressure on the actual area of the contact patch (tread blocks),

- Z_K – measured normal reaction corresponding to the applied load in the wheel axle,
- A_W – the area of the tread blocks contact patch with the rigid ground.

The measurements of the wheel contact patch with the non-deformable ground made it possible to calculate additional auxiliary coefficients [32]:

- tread pattern density coefficient

$$w_{GB} = \frac{A_W}{A_C} \quad (5)$$

- coefficient of the contact patch shape

$$w_{KS} = \frac{l_S \cdot b_S}{A_C} \quad (6)$$

- coefficient of tread blocks loading

$$w_T = \frac{q_{ave}}{p_i} \quad (7)$$

- l_S – the length of the contact patch,
- b_S – the width of the contact patch,
- A_C – total area of the contact patch (defined as the maximum outer envelope of the tread blocks visible in the images of the contact patch, used to determine l_S and b_S),
- p_i – inflation pressure.

The length of the contact patch can also be calculated based on the knowledge of the selected geometric dimensions of the wheel. The first method used (method no. 1) assumes that the length of the contact patch can be calculated on the basis of the knowledge of the outer radius and wheel deflection (fig. 6) and is expressed by a relationship that is commonly used to estimate the length of the contact patch of pneumatic tires [25]:

$$l = 2\sqrt{r_Z \cdot u} \quad (9)$$

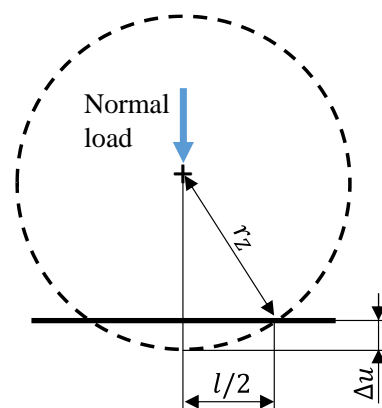


Fig. 6. Tire deformation and contact patch length due to normal load (figure based on [25]).

The second method used to calculate the contact patch length (method no. 2) is presented in [23]. In this model, it was assumed that the radial force increases in a linear manner and is described by the radial stiffness coefficient and can be expressed as the product of the average pressure value and the area of the contact patch [23]:

$$k_{Ri} \cdot u_z = p_{lb} \cdot q \quad (10)$$

- p_{lb} – the rectangular area of the contact patch described by the length l_s and the width b_s ,
- q – the average value of the contact pressure on the rectangular contact patch area.

In this method of estimating the contact patch length, it is assumed that the contact patch area is rectangular, and the contact patch width is similar to the width of the tire (tread

blocks are not taken into account). Equation (10) has been transformed in order to connect to the data that will be measured from the experiment. After substituting equation (6) and assuming that the rectangular contact patch can be replaced with the A_C area, the following expression was obtained:

$$l_s = \frac{k_{Ri} \cdot u_z \cdot WKS}{b_s \cdot q_{aveC}} \quad (11)$$

The average value of the contact pressure resulting from the total contact patch area was also assumed as:

$$q_{aveC} = \frac{ZK}{A_C} \quad (12)$$

The results of the contact patch length calculations using methods 1 and 2 in the "Discussion" section were compared with the results of experimental research.

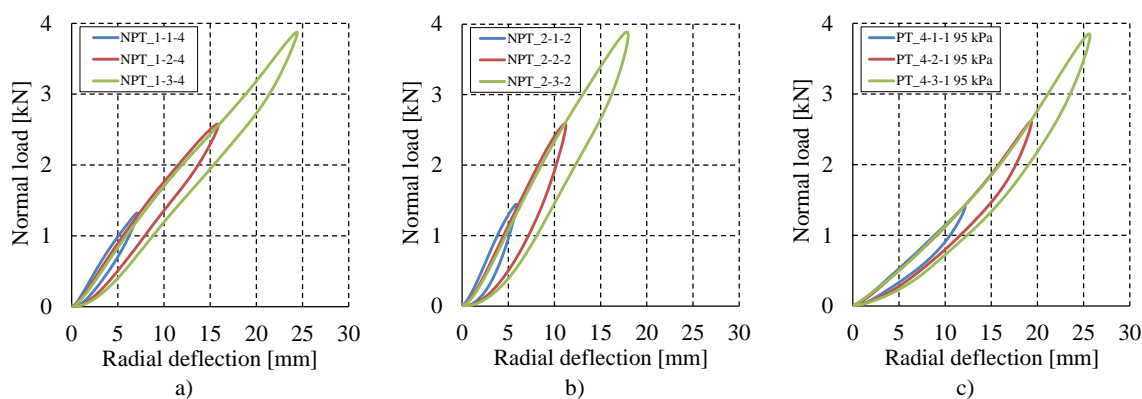


Fig. 7. Example results of radial characteristics experimental research:

a) NPT_1 (cross-section no. 4), b) NPT_2 (cross-section no. 2), c) PT_4 (cross-section no. 1, inflation pressure 95 kPa).

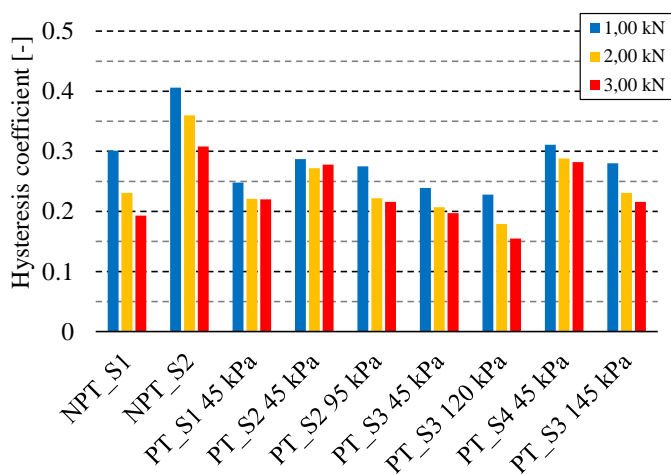


Fig. 8. Calculated values of the hysteresis coefficient of the research objects.

3. Results

Fig. 7 presents the measured radial characteristics for one of the cross-sections of selected wheels during experimental research. Due to the adopted order of tests, the trajectory of the upper curve of the hysteresis loop was converged in subsequent measurements carried out on the same wheel, despite the change in the normal load values.

Fig. 8 presents the hysteresis coefficient values for three normal load values of the tested wheels. The presented results from the tests of pneumatic tires were intentionally limited to the extreme values of the assumed inflation pressure. This limitation results from the need to maintain the legibility of the figure and from the fact that energy losses decreased with the increase of the inflation pressure.

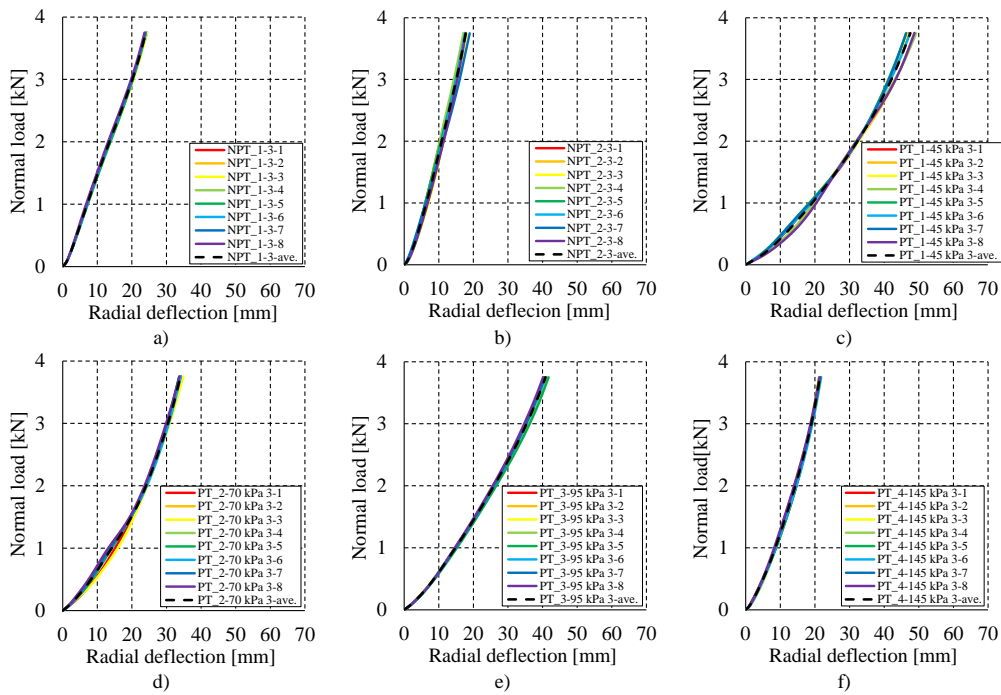


Fig. 9. Example trajectory of the center lines in the analyzed cross-sections (marking 1-8) and the resultant center line:

a) NPT_1, b) NPT_2, c) PT_1 45 kPa, d) PT_2 70 kPa, e) PT_3 95 kPa, f) PT_4 145 kPa.

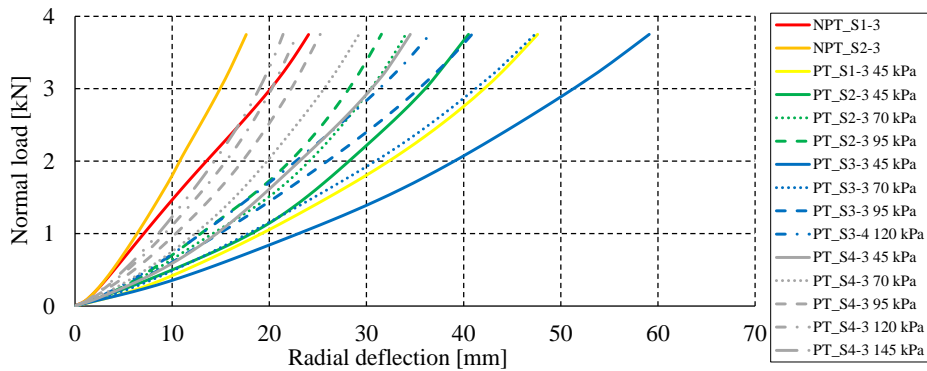


Fig. 10. Comparative summary of the resultant center lines of the research objects radial characteristics.

In the next stage of preparing the results for their analysis, the center line of the hysteresis loop was determined in the set of 8 recorded curves of the radial stiffness characteristics, and then the averaged curve was calculated, shown with a dashed black line in fig. 9. A comparative summary of the averaged (resultant) curves of all wheels is shown in fig. 10.

Fig. 11 shows the changes in the radial stiffness coefficient k_{Ri} of the analyzed wheels with an increase in the normal load value in the range from 0,25 kN to 3,50 kN. Fig. 12 shows the change of the radial stiffness coefficient on the circumference of the wheel corresponding to 100% of the 3,00 kN load (determination of the radial non-uniformity based on 8 measurements made on the circumference of the wheels every 45°).

The values of this coefficient are also shown in table 3 (appendix). Knowledge of this feature will be important in the future in the planned model calculations and in the road experiment carried out in order to determine the motion properties of the vehicle equipped with the tested wheels.

Fig. 18 (appendix) shows the contact patch of the wheels with the non-deformable ground at different values of the normal load. The use of green, red, blue, and gray colors made it possible to show the changes occurring when the normal load was respectively 1,00; 2,00; 3,00; 3,75 kN. The lower intensity shade of the applied color was used to mark total area of the contact patch, determined as a closed area, drawn through the outermost contact points of the tread blocks with the ground.

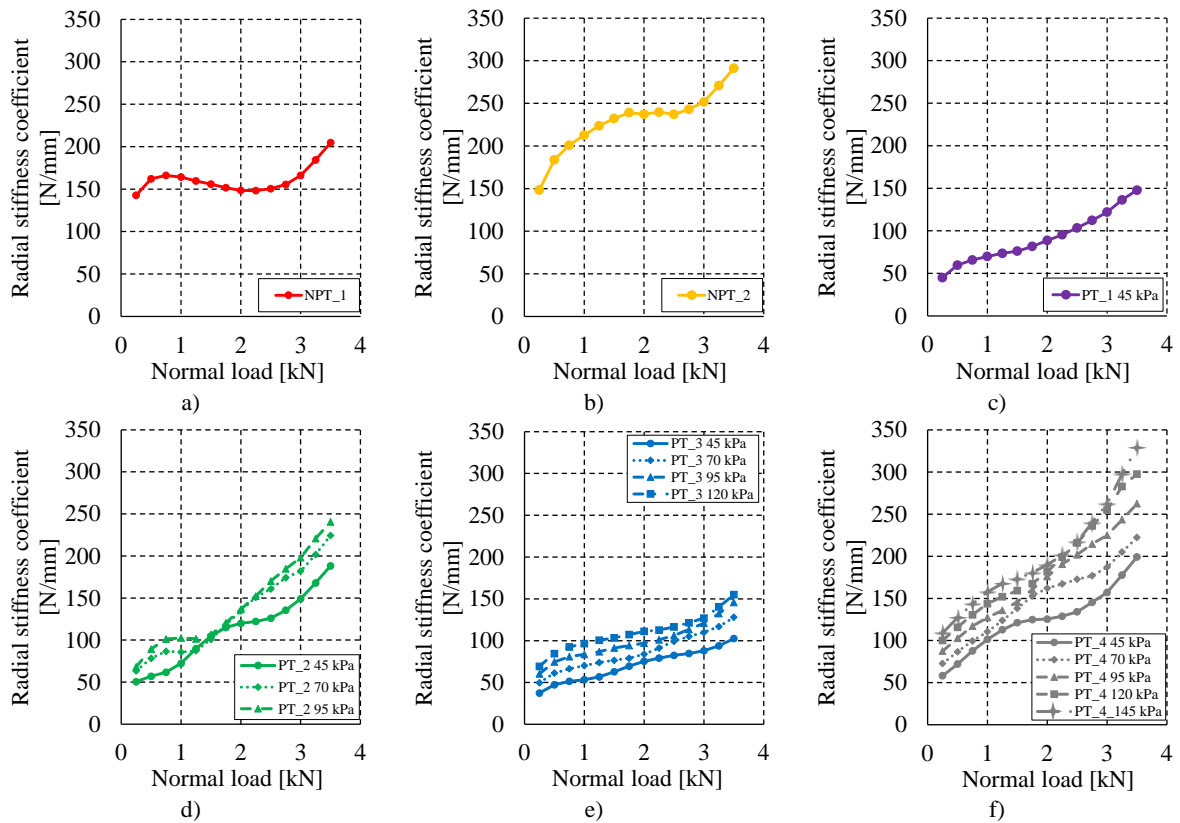


Fig. 11. Changes of radial stiffness coefficient as a function of normal load:

a) NPT_1, b) NPT_2, c) PT_1, d) PT_2, e) PT_3, f) PT_4.

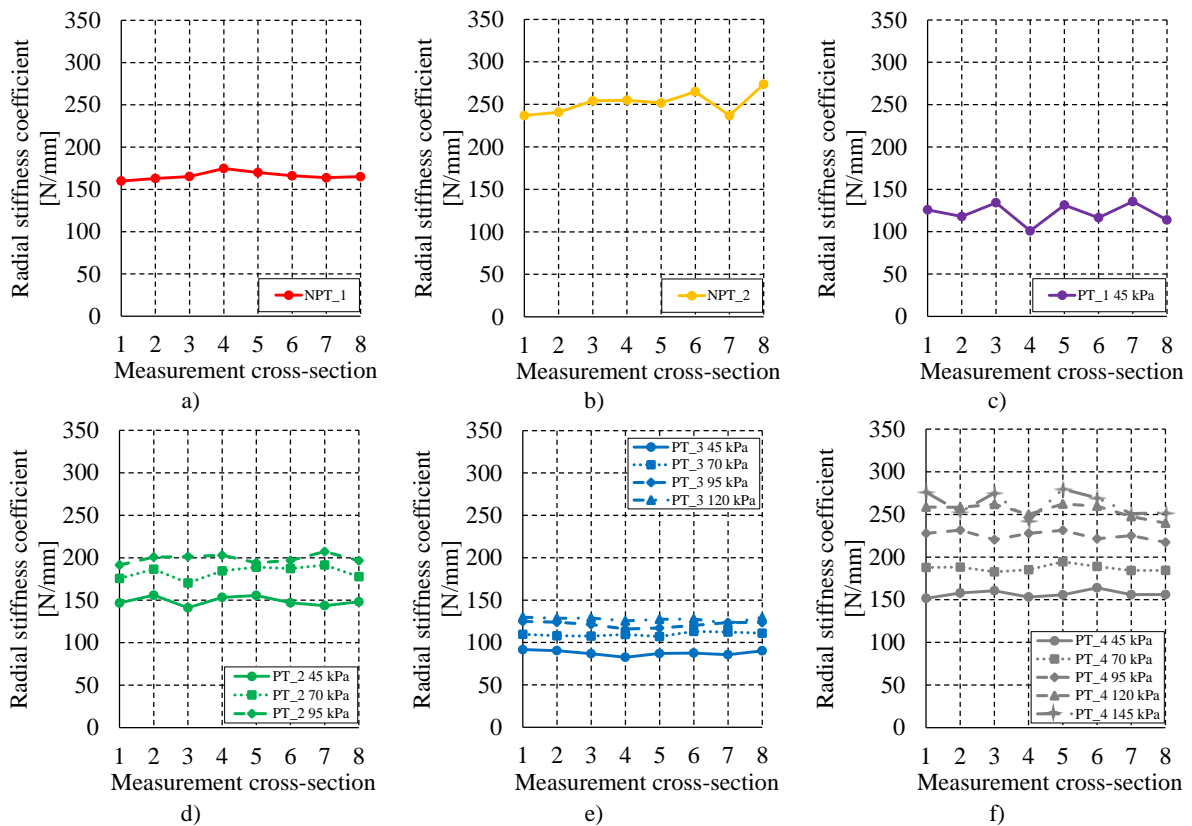


Fig. 12. Changes in the radial stiffness values on the circumference of the analyzed wheels under normal load 3,00 kN:

a) NPT_1, b) NPT_2, c) PT_1, d) PT_2, e) PT_3, f) PT_4.

When determining it, all contact patch measurements under given load conditions in various places around the circumference of the wheel were superimposed. To facilitate the estimation of the contact patch features, a checker section was plotted, where the size of the side of a single (black or white) square is 20 mm.

On the basis of measurements made for two analyzed places (cross-sections) on the circumference of the wheel, the average value of the actual contact area for a given range of normal load was determined. Example results for two locations on the circumference of the tire are shown in fig. 13. Fig. 14 illustrates how the actual contact area of the wheels' changes under the influence of the increase in the normal load. Table 4 (Appendix) lists the values of parameters characterizing the wheel contact patch determined in the research, and fig. 15 shows how the average values of the tread blocks contact pressure were changed.

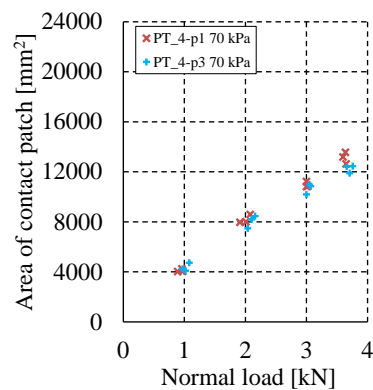


Fig. 13. Exemplary results of contact patch's area measurement as a function of normal load in two sections of the PT_4 (70 kPa).

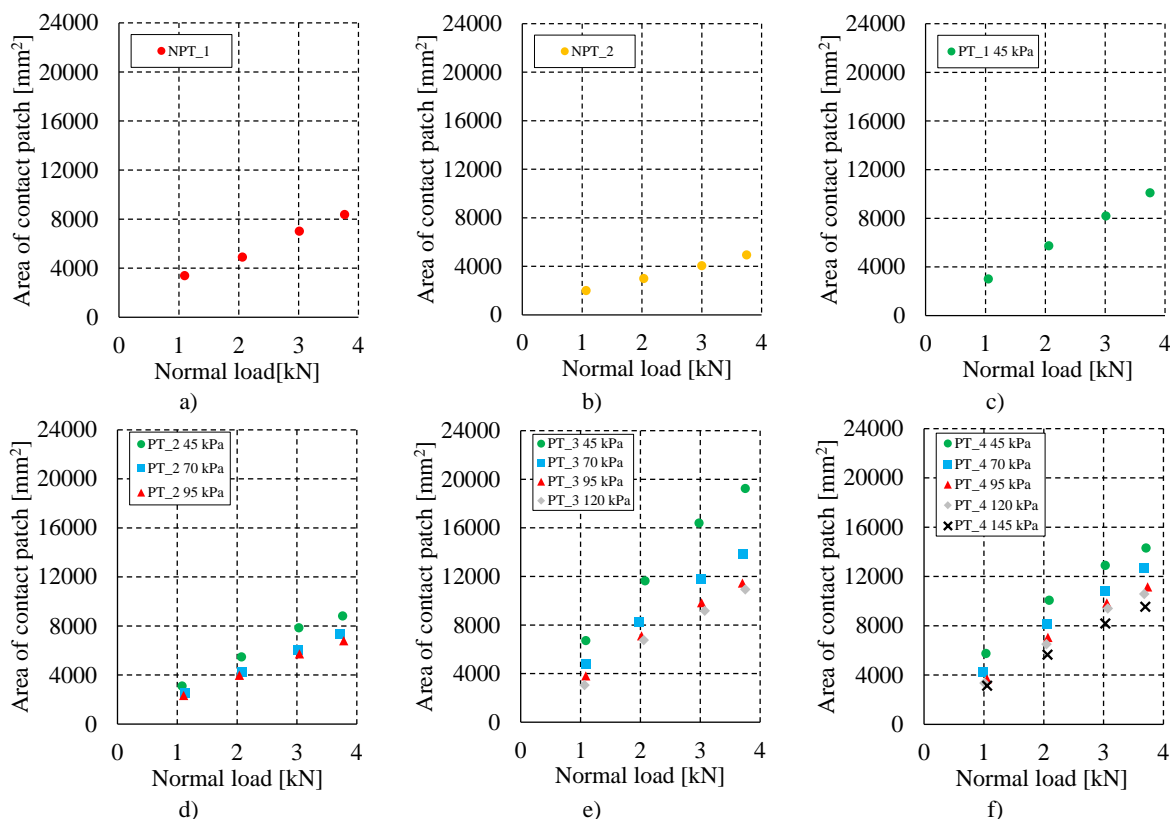


Fig. 14. Change of the area contact patch as a function of normal load: a) NPT_1, b) NPT_2, c) PT_1, d) PT_2, e) PT_3, f) PT_4.

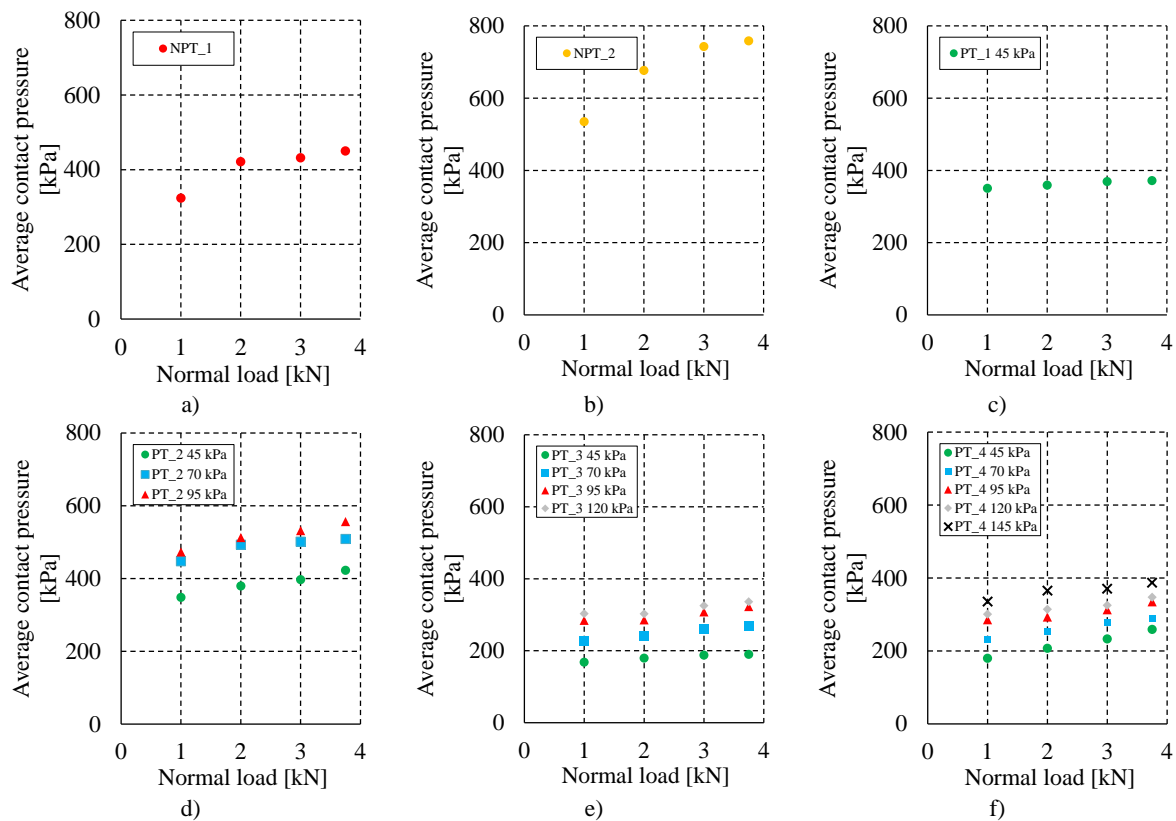


Fig. 15. Change of the contact pressure value in the contact patch of the tread blocks with the non-deformable ground as a function of normal load: a) NPT_1, b) NPT_2, c) PT_1, d) PT_2, e) PT_3, f) PT_4.

4. Discussion

The analysis of direct and indirect wheel research results was divided into three parts. This approach made it possible to systematize the reasoning while revealing the interconnections between the individual areas of consideration.

4.1 Hysteresis - energy losses

The hysteresis recorded during the research of the radial characteristics provided information about the energy losses associated with the vertical deformation of the wheel. In an obvious way, it determines the energy consumption of the rolling wheel (a component of the rolling resistance force), during which cyclical deformations of the wheel occur in the direction normal to the road surface. Energy losses are shown in the form of hysteresis coefficient values (fig. 8). It was observed that the mechanism of vertical loads carrying (resulting, incl., from the type of elastic structure) significantly affects the energy losses of NPTs. Buckling ability of the NPT_1 spokes located between the wheel axis and the contact patch made it possible to achieve values of energy losses close to the values

of energy losses of the analyzed pneumatic tires, i.e. from 19% to 30%. On the other hand, the NPT_2 was characterized by the highest value of the hysteresis coefficient among the analyzed wheels. Depending on the normal load, energy losses ranged from 30% to even 40%. The reason for high energy losses is that, part of the normal load is transferred through the elastic structure located between the NPT_2 axis and the road. Changing the maximum value of the normal load of NPTs resulted in a reduction of energy losses by approx. 10% (almost linear course, reducing losses by 5% for each 1 kN increase in normal load). This direction of changes may be caused by the increasing influence of the increasingly deformed belt with the core and confirms the conclusion presented in [14, 15, 21].

The increase in the inflation pressure of pneumatic tires has obviously resulted in a beneficial reduction in energy losses. Regardless of the inflation pressure of a given pneumatic tire, the value of the hysteresis coefficient changes slightly at 1 kN normal load. The recorded high value of the coefficient at the smallest of the assumed normal loads is caused by the deformation and slip of the massive tread blocks relative to the

ground.

During analyzing the information on the PR index (Ply Rating) of pneumatic tires, it was observed that in the case of the PT_4 (the tire with the highest PR value, table 1), the hysteresis coefficient with the highest value was recorded. This may be due to changes in its load-carrying structure, which consist in the use of additional or reinforced rubber-cord layers. This results in an increase in the volume of material deformed during tire exploitation.

4.2 Radial stiffness

Compared to pneumatic tires, non-pneumatic tires are characterized by a clearly higher radial stiffness and a similar to linear course of the center lines of the radial stiffness characteristics (fig. 10). The NPT_1, equipped with radial spokes, showed significantly lower radial stiffness and lower energy losses during deflection in comparison to the NPT with a hexagonal structure. This is due to a different way of loading the elastic structure, the lower spokes of which are subject to buckling and carry the normal load to a small extent, while the upper spokes (above the wheel axis) are stretched [39]. Observing the changes in the value of the radial stiffness coefficient with the increase in the normal load (fig. 11), the NPTs are characterized by greater non-linearity compared to the courses determined in the research of PTs. The NPT_1 with radial spokes shows an almost constant value of stiffness in the range of low and medium loads (i.e. up to approx. 3,00 kN), while a similar property of the NPT_2 (with a cell structure) occurs in a narrower range of 1,70-2,50 kN. In both analyzed NPTs, a significant increase in the radial stiffness coefficient was observed after exceeding the load of 3,00 kN. The range of changes in the radial stiffness coefficient of NPTs starts from approx. 150 N/mm and reaches a maximum value of approx. 200 N/mm for NPT_1 and approx. 300 N/mm for NPT_2.

The analyzed pneumatic tires, regardless of the value of the inflation pressure, were characterized by progressive characteristics, and the increase in the value of the inflation pressure and normal load resulted in an increase in the value of radial stiffness (fig. 10 and fig. 11). The PTs show significantly lower values of the radial stiffness coefficient at a low normal load. The maximum values of the coefficient (regardless of the inflation pressure) PT_1 and PT_3 reached values below

150 N/mm. Therefore, by comparing only the curve of the radial stiffness of pneumatic tires for the lowest value of inflation pressure, it was observed that PT_3 (radial) had the largest deflection value of approx. 60 mm (the lowest value of radial stiffness coefficient). The bias tires, PT_1 and PT_2, despite significant differences resulting from the load carrying capacity, deflected by approx. 48 mm and 40 mm, respectively. Pneumatic tire PT_4 (radial) for this value of inflation pressure reached a deflection value of approx. 35 mm.

Comparing the analyzed NPT and PT, the PT_4 (radial) tire for the inflation pressure of 120 kPa and 145 kPa had a partially similar curve (of the resultant center line) of the radial characteristics with the NPT_1 (the PT_4 tire had a load carrying capacity higher by approx. 25% compared to the of the analyzed NPTs). The intersection of the aforementioned characteristics occurred at the values of approx. 3,10 kN (deflection of approx. 20 mm) and approx. 2,50 kN (deflection of approx. 17 mm) at the PT_4 inflation pressure of 120 kPa and 145 kPa, respectively. This similarity has already occurred in the values of the discussed hysteresis coefficient.

The radial stiffness coefficients of the analyzed wheels presented in fig. 12 reveal the stiffness non-uniformity on their circumference. The radial stiffness non-uniformity coefficient may indicate inaccuracy of the NPT and PT production or may result from the low density of the tread pattern and the construction of the wheels. Knowing this coefficient can be used in simulation research of a simplified vehicle vertical dynamics model. NPTs achieve a similar value of the radial stiffness coefficient and the radial stiffness non-uniformity coefficient compared to PT_2, PT_3, and PT_4. The PT_1 (low inflation pressure) shows the highest value of the radial stiffness non-uniformity coefficient, which may indicate a significant impact of air pressure on its operational parameters (resulting from the carcass and belt support structure used).

The authors' experience also shows that the non-uniformity of production is difficult to assess for tires with a very low density of the tread pattern built of considerable height blocks. The influence of the tread blocks and the stiffness of the tire's front zone on the non-uniformity of the radial stiffness is particularly visible for the PT_1, whose tread pattern density coefficient is only about 0,23 (the value for off-road tires is usually in the range of 0,40-0,55). The low density of the NPT_2

tread pattern and, additionally, the low value of the allowable inflation pressure for PT_1 resulted in high values of the radial stiffness non-uniformity coefficient achieved in the experiment.

On the basis of the radial characteristics resultant center line curve and the knowledge of the wheel deflection ranges, it is possible to estimate the values of the loads transferred to the vehicle components during its operation. For example, considering the deflection range of analyzed wheels from 5 mm to 15 mm, a change in the force value of approx. can be achieved: NPT_1 – 1,56 kN, NPT_2 – 2,30 kN, PT_1 (45 kPa) – 0,57 kN, PT_2 (45 kPa) – 0,63 kN, PT_2 (95 kPa) – 0,91 kN, PT_3 (45 kPa) – 0,46 kN, PT_3 (120 kPa) – 0,88 kN, PT_4 (45 kPa) – 0,76 kN, PT_4 (145 kPa) – 1,60 kN. The presented estimated range of loads will affect the durability of the vehicle's load-carrying structure and the dynamic load on the vehicle occupant's bodies.

4.3 Contact patch

The analysis of the registered contact patches (fig. 18) made it possible to determine the parameters that were used for their mutual comparison (table 4). The first noticeable feature is that the PTs (compared to NPTs) have always had a longer footprint. The NPT_1 contact patch width, due to the flat shape of the tread front, was practically insensitive to normal load changes. On the other hand, the rounded shape of the NPT_2 tread front (fig. 2b) affected the registered change in the contact patch width with the increase in the normal load. Generalize, in NPTs, the change in the normal load mainly affects the change in contact patch length. In the case of PTs, this influence translates into a change in the length and width of the contact patch. NPT_1 and PT_1-4 at the highest normal load value have the footprint closest to the rectangular shape. The impact of such varied changes in the contact patch on other important wheel motion properties (transferring lateral force and cornering stiffness characteristics) will be checked in subsequent research.

NPT_1 is the only research object for which a greater value of the width than the length of the contact patch was observed (for fixed test conditions). This is due to the flat shape of the tread and the impact of the upper (stretched) spokes of the load-bearing structure, which reduce belt deformations and, as a result, shorten the contact patch (confirmed by the considerations presented in [24]). The shorter contact patch

adversely affects the enveloping properties of the wheel and its resistance to the sideslip. It follows that the knowledge of the contact patch length is the important factor for assessing the wheel co-action with the ground and its impact on the motion parameters of the vehicle equipped with these wheels. This was the reason for comparing two different methods of calculating the contact patch length for the NPTs and the PTs.

The use of method 1 (equation 9) does not allow to calculate the correct value of the contact patch length, especially for NPT_1. A high convergence of experimental results and calculation results of contact patch length was obtained for the calculation method no. 2 described by relation (11). The results of such comparisons are shown in fig. 16. The black "x" mark the experimental results and the orange triangle mark the results of calculation method no. 2.

Another interesting comparison is to show how the actual surface area of the contact patch changes with the increase in the normal load (fig. 14). All analyzed wheels were characterized by a linear change but of different intensity. It was decided to estimate this feature on the basis of the value of the slope of the straight line determined by the method of least squares. According to the comparison made in fig. 17, the lowest intensity of changes occurred in NPTs, for wheels with bias carcass (PT_1 and PT_2) and reinforced radial construction

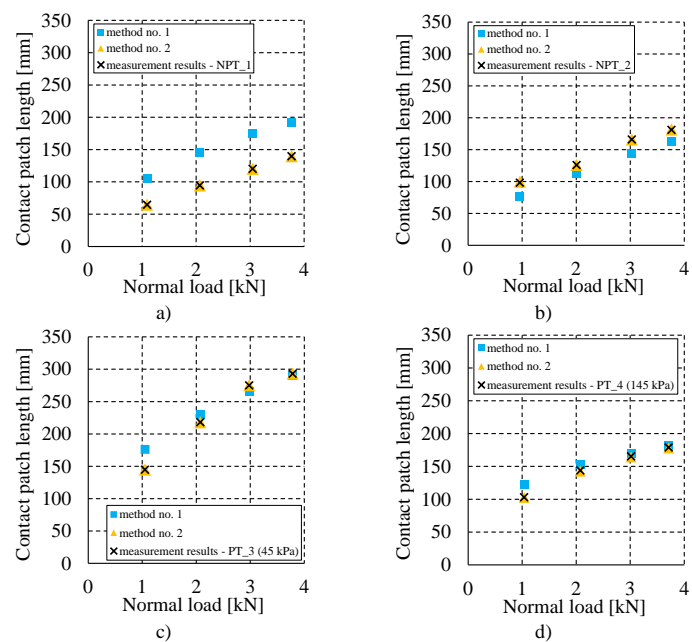


Fig. 16. Comparison of the measured and calculated contact patch lengths of selected wheels: a) NPT_1, b) NPT_2, c) PT_3 (45 kPa), d) PT_4 (145 kPa).

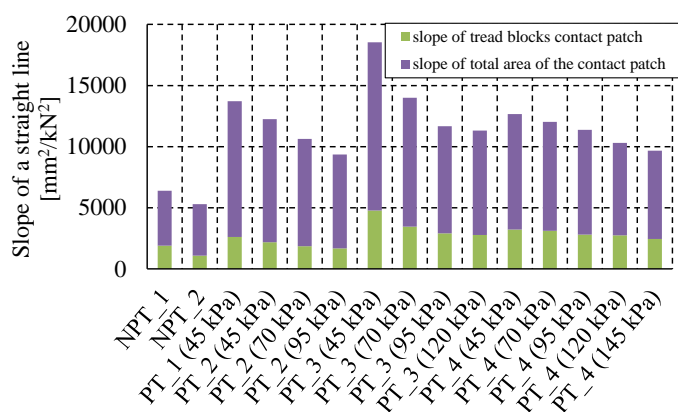


Fig. 17. The measure of the intensity of the changes in the area of contact between the wheels and the rigid ground, caused by an increase in the normal load (in the case of PTs, with each inflation pressure highlighted).

(PT_4) they are similar, while the highest was estimated for the radial tire PT_3. These results coincide with the conclusions formulated in the part concerning the hysteresis assessment (the smallest value of the hysteresis coefficient for the wheel with the highest intensity of changes in the contact area, indicating the largest "participation" of air pressure in the load carrying) and radial stiffness of wheels (an increase in the value of the calculated radial stiffness affects reducing the intensity of the contact area growth).

The low density of the tread pattern shown in fig. 18 and listed in table 4 results from wheels adaptation to the operating conditions of ATVs/UTVs (mainly deformable ground/soft soil). The NPT_1 and the PT_3 and PT_4 (radial tires) have a similar value of the tread pattern density coefficient. A similar group of objects is formed by the NPT_2, the PT_1, and the PT_2 (bias tires), in which the value of the tread density coefficient is definitely lower. This indicates the existing relationship between the radial stiffness of the wheels and the density of the tread pattern.

The pressures in the contact patch of the pneumatic tires tread blocks for a given inflation pressure show slight changes in value with an increase in the normal load (fig. 15). There is a certain regularity here, namely the average pressures calculated for the analyzed bias tires are higher compared to radial tires. An increase in the inflation pressure causes an increase in the contact pressure value and this change is smaller the more the pressure value increases.

In the case of NPTs, the course of change and contact

pressure values are different. The average values of the NPT_2 contact pressure are the highest, which results directly from the smallest contact area of the tread blocks in comparison to the other research objects. In the NPT_1, the average contact pressure values are in the range determined for the bias tires PT_1-2 (whose tread pattern density coefficient was approx. 0,2). An interesting feature of the NPTs is shown in fig. 11a, and 11b as well as 15a, and 15b. In this case, the same character is visible for the wheel radial stiffness curve course change, and the points locations of the contact pressure's average value which are shaped by the increase in the value of the normal load. This feature may be directly related to the tire filling agent (material) forming an elastic structure. This conclusion also results from the observation of changes in the radial stiffness for the lowest inflation pressure value of the objects PT_2 and PT_4 (fig. 11d and 11e), which are tires with the largest volume of material used for their construction. These figures show a portion of characteristic where the increase in the normal load does not change the value of the radial stiffness. A closer explanation of this phenomenon will require more detailed research, also in conditions outside the inflation pressure values adopted in the paper, or even a check on a NPTs numerical models.

Despite the similarities estimated for PTs using the average contact pressure values, clear differences are revealed by another parameter, i.e., the coefficient of tread blocks loading (table 4). It has a significantly lower value (nearly twice) for tires with a radial structure compared to bias tires. A change in the inflation pressure reduces the value of this coefficient in each case, however, the intensity of the decrease and its scope are different again. In the case of bias tires, a constant change was determined, while for radial tires, this change decreases with increasing the inflation pressure.

All these factors taken together show the forecast for the cooperation of the analyzed wheels with a non-deformable (traction and intensity of tread wear) and deformable ground. In this case, the number of the tread blocks hooking edges related to this type of tread pattern with the value of the tread density coefficient, the shape of the tread blocks and the total contact patch area determining the pressure exerted on the ground (parameters partially determined in the described experiment but not yet analyzed) will be additionally important.

5. Conclusions

The paper presents a comparative analysis of the radial stiffness and contact patch of non-pneumatic tires and selected counterparts of pneumatic tires of radial and bias constructions. Manufacturers of NPTs point to the main advantage of these structures, i.e., no need to maintain liquid or gaseous substances under a certain pressure. The load carrying structure used, consisting of the belt and the elastic structure, are components that reflect the properties of compressed air. However, there is no information available on what pressure values they correspond to. Based on the analysis, the following conclusions can be drawn:

1. The type of elastic structure, connecting the wheel rim with the belt (determining the mechanism of carrying vertical loads), will affect the amount of energy losses during vertical deformations of the wheel. These will translate into the rolling resistance force and fuel consumption (it will be checked in the next stages of the research). The elastic cell structure of the NPT_2 caused the greatest energy losses at each of the analyzed load values (hysteresis coefficient value 0,3-0,4). A different shape of the elastic structure in the NPT_1 made it possible to reduce hysteresis losses and bring this structure closer to the properties of pneumatic tires.
2. The radial stiffness characteristics of NPTs correspond to the pneumatic tire with: a) high load carrying capacity, or b) high inflation pressure. This was observed during the analysis of the radial characteristic center lines (fig. 10). The PT_4 for the inflation pressure of 120, and 145 kPa achieved a similar course of characteristics to the NPT_1. It can be expected that a similar relationship can be obtained for other tires inflated above the pressure recommended by the manufacturer.
3. The analyzed NPTs are characterized by low deflection values, which may adversely affect the elements of the suspension system and the load-carrying structure of the vehicle. By analyzing the change in the deflection of the tested objects in a certain range, NPTs obtain a large change

in the value of the radial force. Comparing this range of deflections to the expected range of deflections when driving on rough ground, NPTs can be a source of significant loads, which will also negatively affect driving comfort (vehicle users' loads).

4. The source of driving comfort decreases (at higher speeds) will also be radial non-uniformity, which in the analyzed test objects is mainly due to low density and significant tread blocks.
5. The change in the contact patch width of the NPTs depends on the shape of the tread. The NPTs reached small values of the contact area, which translated into large values of the average contact pressure. Accelerated wear of the NPT can therefore be expected.
6. The use of the radial stiffness coefficient and contact pressures in the contact patch allows for the high results convergence of the contact length calculation and the experiment. It also allows to reveal the interdependencies of these features that were not previously disclosed in the literature analyzed in the review part of the paper.

The research is part of a series of experiments planned and implemented in stages by the authors, which will allow for a detailed comparative analysis of NPTs and PTs and will be used in the process of vehicle motion modeling equipped with NPTs and PTs. Currently, other characteristics of directional stiffness (circumferential, lateral) and rolling of the wheel in the presence of lateral force (cornering) are being researched, which important factors, apart from the inflation pressure, will also be e.g. wheel structure - the inside construction of the pneumatic tire, type and shape of the elastic load-carrying structure and NPT belt as well as the density of the tread pattern.

Authors' contributions and acknowledgements

This work was financed/co-financed by Military University of Technology under research project UGB 763/2022.

References

1. 49 CFR § 571.129 - Standard No. 129; New non-pneumatic tires for passenger cars [<https://www.govinfo.gov/content/pkg/CFR-2014-title49-vol6/pdf/CFR-2014-title49-vol6-sec571-129.pdf>].

2. Ali M, et. al. Design and structural analysis of non-pneumatic tyres for different structures of polyurethane spokes. *Journal of Engineering and Applied Science* 2022, 69 :1-21, 10.1186/s44147-022-00093-5.
3. Choi S J, et al. Non-Pneumatic Tire with Reinforcing Member Having Plate Wire Structure, US 2014/0238561 A1.
4. Cron S, M., Variable Stiffness Spoke For a Non-Pneumatic Assembly. European Patent Office, EP2066502B1.
5. Ganniari-Papageorgiou, E, Chatzistergos P, Wang X, The influence of the honeycomb design parameters on the mechanical behavior of non-pneumatic tires. *Int. J. Appl. Mech.* 2020, 12 (3): 1-15, <https://doi.org/10.1142/S1758825120500246>.
6. Genovese A, Garofano D, Sakhnevych A, Timpone F, Farroni F. Static and Dynamic Analysis of Non-Pneumatic Tires Based on Experimental and Numerical Methods. *Appl. Sci.* 2021, 11, 11232: 1-19, <https://doi.org/10.3390/app112311232>.
7. Hryciów Z, Jackowski J, Żmuda M, The Influence of Non-Pneumatic Tyre Structure on its Operational Properties. *International Journal of Automotive and Mechanical Engineering* 2020, vol. 17, nr 3: 8168-8178, DOI:10.15282/ijame.17.3.2020.10.0614.
8. Hun K Y. Non-Pneumatic Tire Having Improved Riding Comfort, European Patent Specification, EP 2987645B1.
9. Jackowski J, Luty W, Wieczorek M. Oszacowanie oporu toczenia ogumienia 12R22.5. *Biuletyn WAT*, Vol. L, nr 9, pp. 25-36, 2001.
10. Jackowski J, Żmuda M, Wieczorek M, Zuska A. Quasi-Static Research of ATV/UTV Non-Pneumatic Tires. *Energies* 14 (20) 2021, 1-12. <https://doi.org/10.3390/en14206557>.
11. Jin X, Hou C, Fan X, Sun Y, Lv J, Lu C. Investigation on the static and dynamic behaviors of non-pneumatic tires with honeycomb spokes. *Composite Structures* 2018, 187, 27-35, <https://doi.org/10.1016/j.compstruct.2017.12.044>.
12. Kulikowski K, Szpica D. Determination of directional stiffnesses of vehicles' tires under a static load operation. *Maintenance and Reliability* 2014, 16 (1): 66-72.
13. Luty W, Prochowski L, Szurkowski Z. Stanowisko do badań ogumienia dużego rozmiaru. W: VII Międzynarodowe Symp. IPM. Warszawa-Rynia 1999: 375 – 382.
14. Manesh A, et. al. Tension-Based Non-Pneumatic Tire, United States Patent, US 8109308 B2.
15. Manesh A, et. al. Tension-Based Non-Pneumatic Tire, United States Patent, US 8176957 B2.
16. Maxxis® Tires, North American Powersports Catalog, vol. 20. [https://cdn.brandfolder.io/YVLOXW06/at/q4xf8c-7dhf4o-7dxojl/2020_Maxxis_US_pecialty_catalog_lo-res.pdf].
17. Polaris Pro Armour Wheels & Tires. [<https://offroad.polaris.com/en-us/catalogs>].
18. Prochowski L. *Mechanika ruchu*. WKŁ 2008. ISBN : 9788320617016.
19. Regulation No 54 of the Economic Commission for Europe of the United Nations (UNECE) — Uniform provisions concerning the approval of pneumatic tyres for commercial vehicles and their trailers [<https://eur-lex.europa.eu/legal-content/PL/TXT/?uri=CELEX%3A42011X0330%2802%29>].
20. Regulation No 75 of the Economic Commission for Europe of the United Nations (UN/ECE) — Uniform provisions concerning the approval of pneumatic tyres for motor cycles and mopeds [[https://eur-lex.europa.eu/legal-content/EN/TXT/PDF/?uri=CELEX:42011X0330\(02\)](https://eur-lex.europa.eu/legal-content/EN/TXT/PDF/?uri=CELEX:42011X0330(02))].
21. Rhyne T B, Cron S M, Pompier J-P. Compliant Wheel, United States Patent, US 7013939B2.
22. Rhyne T B, DeMino K W, Cron S M, Structurally Supported Resilient Tire. United States Patent, US 6769465B2.
23. Rhyne T B, Development of a Vertical Stiffness Relationship for Belted Radial Tires. *Tire Science and Technology* 2005, 33 (3): 136-155, <https://doi.org/10.2346/1.2174340>.
24. Rhyne T, Cron S, Development of a non-pneumatic wheel. *Tire Sci Technol* 2006; 34(3): 150-169, <https://doi.org/10.2346/1.2345642>.
25. Rill G, Castro A A. *Road Vehicle Dynamics Fundamentals and Modeling with MATLAB®* Second Edition. CRC Press 2020. <https://doi.org/10.1201/9780429244476>
26. Rugsaj R, Suvanjumrat C. Development of a Transient Dynamic Finite Element Model for the Drum Testing of a NonPneumatic Tire. *IOP Conf. Ser.: Mater. Sci. Eng.* 2020 886 012056, 1-8, DOI 10.1088/1757-899X/886/1/012056.
27. Rugsaj R, Suvanjumrat C. Proper Radial Spokes of Non-Pneumatic Tire for Vertical Load Supporting by Finite Element Analysis. *International Journal of Automotive Technology* 2019, 20 (4): 801-812, DOI 10.1007/s12239-019-0075-y.
28. Ružinskas A, Giessler M, Gauterin F, Wiese K, Bogdevičius M. Experimental investigation of tire performance on slush. *Maintenance and Reliability* 2021; 23 (1): 103–109, <http://dx.doi.org/10.17531/ein.2021.1.11>.

29. Terrainarmor Non-Pneumatic Tires. [<https://shop.checkeredflagrecreation.com/polaris-industries-terrainarmor-non-pneumatic-tires-detail.htm?productid=22720982>].
30. The MICHELIN® X® Tweel® Airless Radial Tire Family. [<https://tweel.michelinman.com/>].
31. Thompson R H. Shear Band, United States Patent, US 2010/0018621 A1.
32. Valentin I, Analysis of Tire Contact Parameters Using Visual Processing. *Advances in Tribology* 2010: 1-11, 10.1155/2010/491723.
33. Vinay T V, Marattukalam K J, Varghese S Z, Samuel S, Sreekumar S. Modeling and Analysis of Non-Pneumatic Tyres with Hexagonal Honeycomb Spokes. *International Journal on Recent Technologies in Mechanical and Electrical Engineering (IJRMEE)* 2015, Volume: 2 Issue: 3: 019 – 024, ISSN: 2349-7947.
34. Xu T, Yang J, Zhu L, Gao F. Lightweight Design Optimization of Nonpneumatic Tires under Radial-Stiffness Constraints. *Machines* 2022, 10 (10), 889: 1-16, <https://doi.org/10.3390/machines10100889>.
35. Yaoji D, Zhiyue W, Hui S, Junjie G, Zhen X. A comprehensive review on non-pneumatic tyre research. *Materials & Design* 2023, 227, 1-22, <https://doi.org/10.1016/j.matdes.2023.111742>.
36. Zhang Z, Fu H, Liang X, Chen X, Tan D. Comparative Analysis of Static and Dynamic Performance of Nonpneumatic Tire with Flexible Spoke Structure. *Strojniški vestnik - Journal of Mechanical Engineering* 2020, 66: 458-466, 10.5545/sv-jme.2020.6676.
37. Zhao Y, Du X, Lin F, Wang Q, Fu H. Static stiffness characteristics of a new non-pneumatic tire with different hinge structure and distribution. *J. Mech. Sci. Technol.* 2018, 32: 3057–3064, DOI 10.1007/s12206-018-0608-8.
38. Zheng Z, Rakheja S, Sedaghati R. Multi-axis stiffness and road contact characteristics of honeycomb wheels: A parametric analysis using Taguchi method. *Composite Structures* 2022, 279, 114735, 1-14, <https://doi.org/10.1016/j.compstruct.2021.114735>.
39. Żmuda M, Construction analysis of non-pneumatic tires. *Biuletyn WAT* 2021, 70 (1): 113-128, DOI:10.5604/01.3001.0015.6962.
40. Żuchowski A. Analiza wpływu niejednorodnych właściwości kół jezdnych na drgania samochodu. PhD thesis, Warszawa 2002.

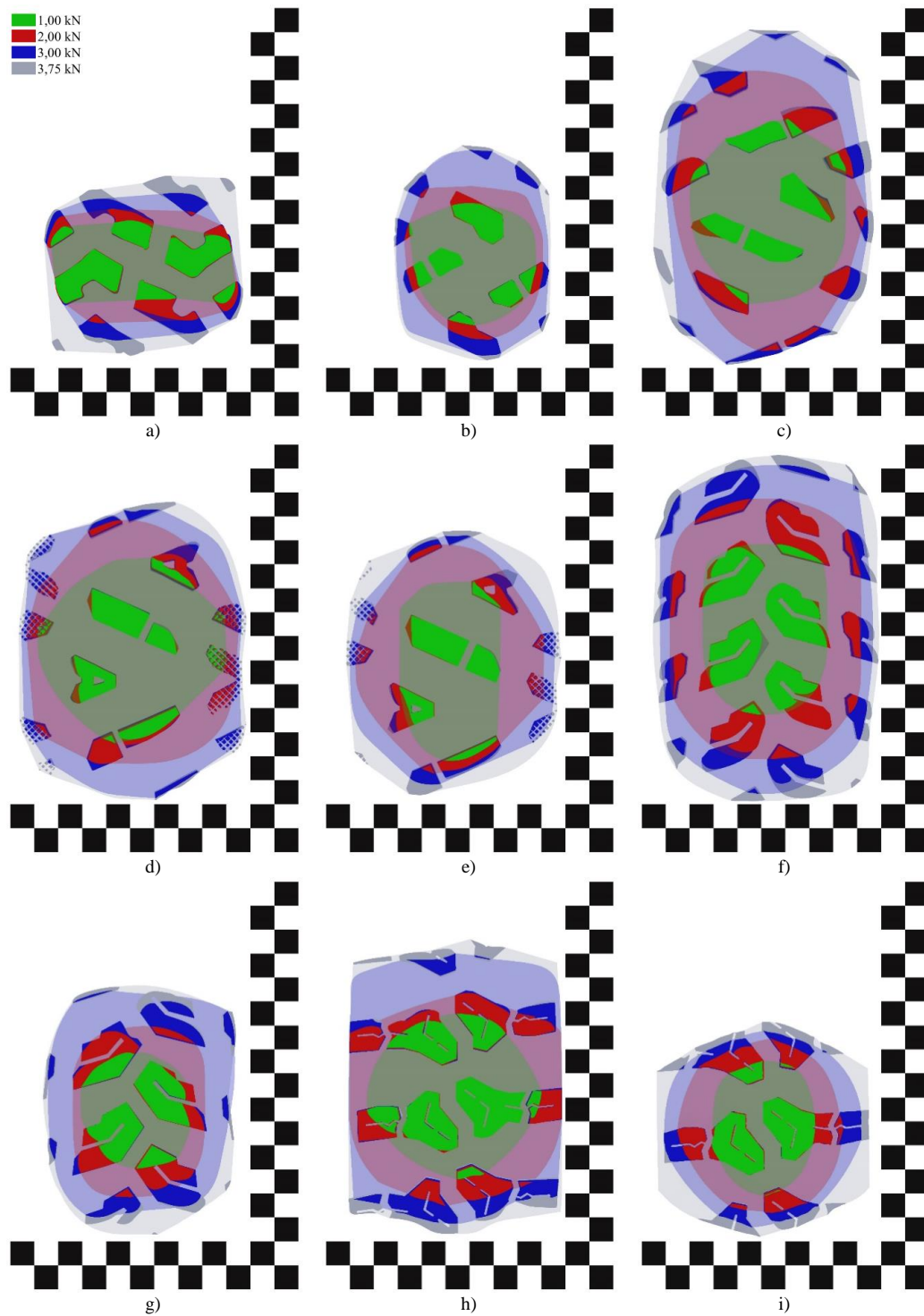


Fig. 18. Contact patch with the non-deformable ground:

- a) NPT_1, b) NPT_2, c) PT_1 (45 kPa), d) PT_2 (45 kPa), e) PT_2 (95 kPa),
 f) PT_3 (45 kPa), g) PT_3 (120 kPa), h) PT_4 (45 kPa), i) PT_3 (145 kPa).

Table 3. Values of the radial stiffness coefficient of the research objects for a load of 3,00 kN calculated at the point corresponding to 100% of the normal load (according to the explanation shown in fig. 4).

Wheel	Radial stiffness coefficient [N/mm]									Radial stiffness non-uniformity coefficient [%]
	1	2	3	4	5	6	7	8	Average	
NPT_1	159,96 ±1,04	163,01 ±0,76	165,21 ±1,08	174,75 ±1,40	170,02 ±1,73	166,14 ±2,87	163,83 ±0,55	165,17 ±1,55	166,01 ±4,25	8,91
NPT_2	236,82 ±1,86	240,80 ±5,18	254,15 ±1,60	254,86 ±3,78	251,68 ±4,14	264,90 ±3,05	236,91 ±0,80	273,63 ±0,89	251,72 ±12,4	14,62
PT_1 45 kPa	125,85 ±1,80	117,95 ±0,41	134,15 ±0,18	101,01 ±0,82	131,44 ±0,63	116,53 ±0,42	135,65 ±0,84	113,86 ±1,20	122,06 ±11,13	28,38
PT_2 45 kPa	146,82 ±0,95	155,89 ±3,76	141,05 ±1,16	153,33 ±2,25	155,69 ±6,83	146,98 ±1,00	143,68 ±6,66	148,16 ±0,63	148,95 ±5,15	9,96
PT_2 70 kPa	175,59 ±2,68	186,45 ±5,43	170,37 ±0,01	184,52 ±0,62	188,99 ±0,34	187,27 ±4,35	191,51 ±0,12	177,75 ±2,11	182,81 ±6,91	11,56
PT_2 95 kPa	191,50 ±1,82	200,84 ±1,86	201,30 ±0,61	203,11 ±0,30	194,14 ±1,25	196,72 ±2,59	207,22 ±0,47	196,57 ±2,54	198,93 ±4,8	7,90
PT_3 45 kPa	91,68 ±0,89	90,47 ±0,21	86,76 ±0,53	82,59 ±0,83	87,12 ±0,04	87,53 ±0,34	85,68 ±0,34	90,25 ±0,41	87,76 ±2,77	10,36
PT_3 70 kPa	109,76 ±0,31	107,99 ±1,10	107,61 ±1,10	109,51 ±0,88	106,97 ±0,39	113,18 ±0,32	112,40 ±0,56	111,09 ±1,27	109,81 ±2,12	5,66
PT_3 95 kPa	124,86 ±2,70	123,94 ±1,82	121,23 ±2,62	115,94 ±1,80	117,06 ±3,52	120,14 ±0,59	123,52 ±1,27	123,52 ±0,77	121,28 ±3,11	7,36
PT_3 120 kPa	129,94 ±0,80	128,59 ±1,23	128,95 ±3,37	125,57 ±0,69	127,47 ±1,51	127,84 ±1,23	122,55 ±0,32	129,51 ±2,79	127,55 ±2,28	5,79
PT_4 45 kPa	151,63 ±1,66	157,92 ±0,59	160,56 ±0,95	153,18 ±0,55	155,73 ±0,83	164,03 ±1,16	155,94 ±0,38	156,10 ±2,15	156,89 ±3,70	7,90
PT_4 70 kPa	187,92 ±2,63	188,32 ±1,19	182,69 ±0,54	185,22 ±2,45	194,55 ±1,11	189,07 ±0,94	184,21 ±1,09	184,39 ±2,19	187,05 ±3,54	6,34
PT_4 95 kPa	227,76 ±1,06	231,59 ±0,63	220,33 ±1,54	227,87 ±1,08	231,37 ±1,18	221,52 ±1,00	225,08 ±1,33	217,36 ±1,56	225,36 ±4,89	6,31
PT_4 120 kPa	258,69 ±0,25	258,37 ±1,17	261,85 ±1,22	250,12 ±1,74	262,28 ±1,28	259,83 ±0,84	247,60 ±1,99	239,82 ±0,51	254,82 ±7,56	8,81
PT_4 145 kPa	276,19 ±1,22	252,97 ±0,74	275,07 ±0,21	242,64 ±0,47	279,78 ±0,45	269,47 ±0,97	250,98 ±1,32	252,00 ±1,12	262,39 ±13,33	14,15

Potential NPT substitutes by PT in the assumed normal load range are marked with colors.

Table 4. The parameters determined in the research characterizing the contact patch
with the non-deformable ground of the analyzed wheels

Normal load [kN]	Area of contact patch [m ²]	Tread pattern density coefficient [-]	Contact length [m]	Contact length – method no. 2[m]	Contact width [m]	Coefficient of the contact patch shape [-]	Average contact pressure [kPa]	Coefficient of tread blocks loading [-]
NPT_1								
1,00	0,00339 ±0,00018	0,41 ±0,01	0,065 ±0,004	0,065 ±0,005	0,145 ±0,009	1,081 ±0,064	307,01 ±16,18	-
2,00	0,00490 ±0,00030	0,41 ±0,01	0,095 ±0,002	0,095 ±0,002	0,159 ±0,001	1,212 ±0,004	442,81 ±10,25	-
3,00	0,00697 ±0,00018	0,42 ±0,01	0,120 ±0,001	0,120 ±0,001	0,160 ±0,002	1,179 ±0,017	432,16 ±11,03	-
3,75	0,00837 ±0,00011	0,40 ±0,01	0,140 ±0,001	0,140 ±0,001	0,168 ±0,002	1,118 ±0,018	450,06 ±3,34	-
NPT_2								
1,00	0,00201 ±0,00016	0,27 ±0,02	0,098 ±0,003	0,100 ±0,013	0,100 ±0,004	1,354 ±0,069	535,13 ±39,76	-
2,00	0,00300 ±0,00018	0,28 ±0,01	0,126 ±0,003	0,126 ±0,005	0,116 ±0,003	1,327 ±0,044	676,93 ±29,29	-
3,00	0,00404 ±0,00019	0,25 ±0,01	0,166 ±0,004	0,166 ±0,003	0,125 ±0,002	1,280 ±0,048	743,04 ±23,54	-
3,75	0,00495 ±0,00013	0,26 ±0,01	0,181 ±0,001	0,182 ±0,003	0,131 ±0,001	1,268 ±0,039	758,47 ±19,60	-
PT_1 – 45 kPa								
1,00	0,00301 ±0,00029	0,24 ±0,01	0,154 ±0,005	0,154 ±0,003	0,121 ±0,007	1,494 ±0,093	350,82 ±16,92	7,80 ±0,38
2,00	0,00574 ±0,00040	0,22 ±0,01	0,232 ±0,002	0,232 ±0,002	0,157 ±0,007	1,399 ±0,038	359,29 ±19,10	7,98 ±0,42
3,00	0,00815 ±0,00016	0,22 ±0,01	0,276 ±0,001	0,276 ±0,003	0,174 ±0,003	1,266 ±0,014	369,41 ±12,74	8,21 ±0,28
3,75	0,01009 ±0,00024	0,24 ±0,01	0,280 ±0,001	0,280 ±0,003	0,185 ±0,001	1,235 ±0,003	371,76 ±10,60	8,26 ±0,24
PT_2 – 45 kPa								
1,00	0,0031 ±0,00014	0,19 ±0,01	0,155 ±0,001	0,155 ±0,004	0,157 ±0,003	1,431 ±0,024	348,38 ±14,82	7,74 ±0,33
2,00	0,00547 ±0,00035	0,19 ±0,01	0,208 ±0,005	0,208 ±0,008	0,178 ±0,002	1,294 ±0,061	379,42 ±13,34	8,43 ±0,30
3,00	0,00759 ±0,00065	0,19 ±0,01	0,246 ±0,006	0,247 ±0,006	0,186 ±0,002	1,217 ±0,018	397,11 ±24,12	8,52 ±0,13
3,75	0,00882 ±0,00068	0,19 ±0,01	0,262 ±0,014	0,263 ±0,007	0,192 ±0,002	1,174 ±0,013	422,68 ±24,42	9,13 ±0,14
PT_2 – 95 kPa								
1,00	0,00234 ±0,00017	0,21 ±0,01	0,150 ±0,001	0,150 ±0,002	0,083 ±0,002	1,129 ±0,032	473,04 ±21,09	4,98 ±0,22
2,00	0,00398 ±0,00016	0,18 ±0,01	0,191 ±0,001	0,191 ±0,003	0,158 ±0,001	1,401 ±0,02	512,47 ±13,81	5,39 ±0,15
3,00	0,00573 ±0,00015	0,21 ±0,01	0,210 ±0,001	0,210 ±0,002	0,174 ±0,001	1,324 ±0,013	531,63 ±23,96	5,60 ±0,25
3,75	0,00679 ±0,00006	0,21 ±0,01	0,222 ±0,001	0,222 ±0,002	0,179 ±0,001	1,224 ±0,038	556,45 ±5,17	5,86 ±0,05
PT_3 – 45 kPa								
1,00	0,00672 ±0,00077	0,43 ±0,01	0,145 ±0,002	0,145 ±0,007	0,106 ±0,001	1,139 ±0,008	168,63 ±11,17	3,75 ±0,25
2,00	0,01163 ±0,00095	0,35 ±0,01	0,218 ±0,001	0,218 ±0,003	0,161 ±0,001	1,164 ±0,023	179,66 ±14,6	3,99 ±0,32
3,00	0,01622 ±0,00095	0,35 ±0,01	0,275 ±0,001	0,275 ±0,002	0,178 ±0,001	1,129 ±0,021	187,85 ±11,79	4,17 ±0,26

3,75	0,01924 ±0,00095	0,36 ±0,01	0,293 ±0,004	0,293 ±0,004	0,191 ±0,002	1,107 ±0,011	190,37 ±7,09	4,23 ±0,16
PT_3 – 120 kPa								
1,00	0,00365 ±0,00046	0,48 ±0,01	0,103 ±0,006	0,107 ±0,003	0,097 ±0,005	1,224 ±0,017	303,27 ±16,6	2,53 ±0,14
2,00	0,00675 ±0,00062	0,46 ±0,01	0,150 ±0,005	0,150 ±0,002	0,113 ±0,002	1,103 ±0,025	302,94 ±13,88	2,52 ±0,12
3,00	0,00945 ±0,00064	0,38± 0,02	0,192 ±0,003	0,192 ±0,003	0,157 ±0,005	1,154 ±0,026	325,44 ±11,01	2,71 ±0,09
3,75	0,01092 ±0,00068	0,38 ±0,01	0,212 ±0,004	0,212 ±0,003	0,164 ±0,002	1,173 ±0,016	336,26 ±13,37	2,80 ±0,11
PT_4 – 45 kPa								
1,00	0,00576 ±0,0004	0,38 ±0,01	0,137 ±0,001	0,138 ±0,002	0,155 ±0,008	1,367 ±0,029	180,14 ±12,93	4,00 ±0,29
2,00	0,01007 ±0,00017	0,38 ±0,01	0,179 ±0,001	0,179 ±0,003	0,178 ±0,001	1,211 ±0,013	207,56 ±2,73	4,61 ±0,06
3,00	0,01299 ±0,00034	0,35 ±0,01	0,231 ±0,003	0,231 ±0,003	0,179 ±0,001	1,108 ±0,001	233,10 ±8,29	5,18 ±0,18
3,75	0,01431 ±0,00021	0,36 ±0,01	0,249 ±0,002	0,249 ±0,003	0,179 ±0,001	1,110 ±0,005	258,96 ±2,65	5,75 ±0,06
PT_4 – 145 kPa								
1,00	0,00314 ±0,00021	0,44 ±0,03	0,107 ±0,009	0,107 ±0,003	0,086 ±0,004	1,250 ±0,019	335,65 ±15,6	2,31 ±0,11
2,00	0,00565 ±0,00035	0,37 ±0,01	0,143 ±0,002	0,143 ±0,001	0,131 ±0,006	1,300 ±0,014	365,50 ±16,29	2,52 ±0,11
3,00	0,00818 ±0,00030	0,37 ±0,01	0,165 ±0,001	0,166 ±0,003	0,167 ±0,001	1,267 ±0,036	370,55 ±9,91	2,56 ±0,07
3,75	0,00955 ±0,00008	0,37 ±0,01	0,178 ±0,002	0,178 ±0,001	0,178 ±0,001	1,213 ±0,006	387,21 ±7,33	2,67 ±0,05